Current Plant Biology 39 (2024) 100356

Contents lists available at ScienceDirect

Current Plant Biology

journal homepage: www.elsevier.com/locate/cpb

Triangle area model (*TAM*) for predicting germination: An approach to enhance hydrothermal time model applications

Mostafa Oveisi [a,*], Hassan Alizadeh [a], Sassan A. Lorestani [a], Aboozar Esmaili [a], Nasrin Sadeghnejad [a], Ramin Piri [a], Jose L. Gonzalez-Andujar [a,b], Heinz Müller-Schärer [a,c,**]

[a] Department of Agronomy and Plant Breeding, College of Agriculture and Natural Resources, University of Tehran, Karaj, Iran
[b] Department of Crop Protection, Institute for Sustainable Agriculture (CSIC), Cordoba 14004, Spain
[c] Department of Biology, University of Fribourg, Fribourg, Switzerland

ARTICLE INFO

Keywords:
Triangle area model
Sub-optimal temperature
Supra-optimal temperatures
Hydrothermal time germination
Ambrosia psilostachya L.
Cynanchum acutum L.
Bidens pilosa L

ABSTRACT

A thorough examination of assumptions in hydrothermal time models revealed areas for enhancing model performance. We introduce the Triangle Area Model (*TAM*), which uses the area of right-angled triangles to calculate hydrothermal time for predicting population germination fractions (g). TAM is characterized by its depiction of triangles, considering insightful parameters such as the distance of germination temperature (T) to the base (T_b), optimal (T_o), and ceiling (T_c) temperatures, the range of $T_c - T_o$, $T_o - T_b$, and the germination water potential (Ψ), i.e. mean base water potential ($\Psi_{b(g)}$), along with potential g that may occur with T and Ψ combinations within $T_c - T_b$ when $\Psi > \Psi_{b(g)}$. Applied to germination data from *Ambrosia psilostachya* L., *Cynanchum acutum* L., and *Bidens pilosa* L., *TAM* achieves an *RMSE* of 0.03 for *A. psilostachya* and *C. acutum*, and 0.05 for *B. pilosa*. Moreover, *TAM* demonstrates an R^2 of 0.96, 0.97, and 0.98 for the respective species. *TAM* significantly outperforms earlier models through a comparison with varying T and Ψ. *TAM* determined T_b for *A. psilostachya*, *C. acutum*, and *B. pilosa* as 0.19, 14.57, and 5.76 °*C*; T_o as 25.1, 39.9, and 29.8 °*C*; and T_c as 46.7, 53, and 41°*C*, for the respective species. It also estimates $\Psi_{b(g)}$ as -1.48 for *A. psilostachya*, -0.98 for *C. acutum*, and -0.97 for *B. pilosa*. The *TAM* approach deepens our understanding of temperature-moisture processes influencing plant survival, colonization, and habitat expansion for these three invasive alien species. Furthermore, it can be more widely applied for estimating *TT* and *HTT* across different growth stages, enhancing the prediction accuracy of plant phenological development.

1. Introduction

Seed germination is a critical stage in plant growth, ensuring the emergence and establishment of seedlings and initiating the plant life cycle. Understanding its mechanism is paramount for accurately predicting plant development, growth, and fecundity [48]. Water holds a crucial role in seed germination by providing the necessary hydration for protoplasmic activities, supplying dissolved oxygen to the growing embryo, softening seed coats, and enhancing seed permeability. Additionally, it facilitates the breakdown of seed dormancy, converting insoluble food into a soluble form for translocation to the embryo [7]. The success of seed germination relies on species-specific favorable temperatures spanning from a base temperature (T_b) to a ceiling temperature (T_c). However, water and temperature interact intricately, where alterations in one can influence the magnitude of the other's impact [41].

Hydrothermal time models, extensively employed in predicting germination, consider the interactive effects of water potential and temperature over time [6]. Gummerson [17] introduced a model correlating the time of germination with a fraction of germination (g), denoted as $t_{(g)}$. This correlation remains valid as long as the constant water potential (Ψ) and suboptimal temperature (T) of each seed surpass specific thresholds (Ψ_b and T_b, respectively), below which germination cannot take place. Mathematically, this hydrothermal time (*HTT*) can be calculated as:

$$HHT = (\Psi - \Psi_b) \times (T - T_b) \times t_{(g)} \quad (1)$$

Consequently, when estimating *HTT* under sub-optimal

* Corresponding author.
** Corresponding author at: Department of Agronomy and Plant Breeding, College of Agriculture and Natural Resources, University of Tehran, Karaj, Iran.
E-mail addresses: moveisi@ut.ac.ir (M. Oveisi), heinz.mueller@unifr.ch (H. Müller-Schärer).

https://doi.org/10.1016/j.cpb.2024.100356
Received 14 January 2024; Received in revised form 8 March 2024; Accepted 23 May 2024
Available online 24 May 2024
2214-6628/© 2024 The Authors. Published by Elsevier B.V. This is an open access article under the CC BY-NC license (http://creativecommons.org/licenses/by-nc/4.0/).

temperatures, two sub-functions come into play. Thermal units can be computed by subtracting the species' base temperature from the experimental temperature. Similarly, hydro units can be determined by subtracting the species' base water potential from the experimental water potential. By multiplying these resulting thermal and hydro units by the time to any given germination fraction (g), the *HTT* to g is derived [10]. However, subtracting the base temperature (T_b) from the ambient temperature applies to any T within the range of T_b to T_c [17], resulting in an increase in thermal time even when T approaches T_c. It would be reasonable to assume that the highest *TT* should correspond to the optimal temperature. To address this concern, Bradford, [10] implemented adjustments aimed at preventing an excessive rise in *TT* during supra-optimal temperature. He achieved this by subtracting T_b from T_o under such conditions. However, when seeds germinate at T near T_c, the computed *TT* remains identical to that of seeds germinating at the optimal T. Furthermore, Alvarado and Bradford, [3] and Rowse and Finch-Savage, [36] explicitly dealt with the impact of supra-optimal T on the base water potential. To account for this effect, a coefficient was introduced to multiply (T - T_o). The resulting value was then added to the mean base water potential of the seed population. Thus, as T approaches T_c, the base water potential shifts towards less negative values, effectively controlling the increase of *TT*, and accordingly, *HTT* over T greater than T_o. Efforts to enhance the model's applications, including probit-based models relating to proportional germination [18], incorporating stochasticity through the sensitive parameters of hydrothermal time models using various distribution functions [28], hydrothermal-time-to-event models [31], and population-based threshold (PBT) models [11,21], have further improved the applicability of hydrothermal time germination models. However, these approaches rely on specific assumptions, such as the normality of data or continuous germination observations over time. Deviations from these assumptions may lead to the models failing to perform effectively [18]. Nevertheless, revisiting the methods for estimating *HTT* could still yield new insights that may further enhance the applicability of *HTT* models [8].

A careful analysis of the assumptions in the *HTT* models brings to light opportunities for improvement in the approaches used for estimating *HTT*. For instance, the assumption of a linear increase in thermal time (*TT*) to g for temperatures below T_o might not hold true from a biological standpoint. As an example, if T_b and T_o of a plant are 2 and 20 $^\circ C$, respectively, the current assumption implies that increasing T from 2 to 3 $^\circ C$ has the same effect as increasing T from 12 to 13$^\circ C$. Similarly, the oversight of the decrease in *TT* with supra-optimal temperatures is another area where the current linear decrease assumption does not hold true. It assumes the same decreasing effect of increasing T for temperatures close to T_o and T_c, while seeds germinating at or slightly above the base temperature, as well as those germinating at temperatures near T_c, differ from seeds germinating around optimal temperatures in their ability to accumulate *TT*.

From a physiological perspective, thermo-inhibition plays a crucial role in determining the germination capacity of seeds and the rate at which this process occurs [19]. This phenomenon is significantly influenced by phytohormones such as ethylene, abscisic acid (*ABA*), and gibberellins (*GA*). Consequently, a one-degree increase in temperature for seeds near T_b or T_c, compared to those close to T_o could yield different effects. At lower temperatures, there could be notable decreases in chlorophyll and carotenoid content, as well as reduced activities of enzymes like peroxidase, superoxide dismutase, and catalase. It is also proven that at temperatures around T_b, the levels of electrolyte leakage, malondialdehyde, hydrogen peroxide, and superoxide radicals increased [16]. Consequently, seeds at lower temperatures encounter bio-chemo-physical limits in responding to ambient factors, including temperature. Conversely, seeds germinating at T_o demonstrate greater physiological responsiveness to ambient temperature.

Similar arguments can be extended to the impact of water potential. The uptake of water by mature dry seeds follows a triphasic pattern: rapid initial uptake (*phase I*, imbibition) followed by a plateau phase (*phase II*, metabolic preparation for germination), and further water uptake immediately after germination *(phase III)*, resulting in hydraulic growth of the embryo and the emerged seedling. The presence of the plant hormone *ABA* inhibits *phase III* water uptake [23]. When seeds exceed critical water contents, the ambient water potential significantly influences the rate of seed germination through hormonal regulation. Seeds germinating slightly above Ψ_b can remain inhibited by *ABA*, whereas seeds exposed to adequate moisture are relieved from *ABA*'s inhibitory effects. Consequently, an increase in ambient moisture does not produce uniform effects on seeds around the base water potential and seeds germinating under sufficient moisture conditions [15]. In essence, higher available moisture meets the primary needs of seeds and can directly expedite the germination rate [5].

These variable responses concerning *TT*, *HT*, and *HTT* are further complicated by the interaction of hydrothermal time. The impacts of water absorption, imbibition, and subsequent moisture-related stages on seed germination are bio-physical [34], with significant dependency on the ambient temperature [43]. Consequently, the effect of moisture on seeds maintained at the base or ceiling temperature may vastly differ from that observed at optimal temperatures.

In the current study, we propose modifications to *HTT* calculations addressing the following main issues: 1) the increasing effect of $T_n - T_{n-1}$ should not be uniform for temperatures within $T_o - T_b$. Specifically, increasing T near T_o should have a higher impact than lower T near T_b, 2) the decreasing effect of $T_n - T_{n-1}$ should not be uniform for temperatures within $T_c - T_o$, in particular, increasing T near T_c should have a more pronounced negative effect than lower T near T_o, and 3) the increasing effect of $\Psi_n - \Psi_{n-1}$ should not be the same for water potential near Ψ_b and those of sufficient moisture for germination. To address the aforementioned issues, we have adopted a novel approach for calculating *HTT*. This approach employs a right-angled triangle model to calculate *TT*, *HT*, and *HTT*. It considers the germination fraction at each T or Ψ, as well as the distance of temperature from T_o and water potential from Ψ_b. We then test our model using three datasets from germination experiments with *Ambrosia psilostachya* L. DC, *Cynanchum acutum* L., and *Bidens pilosa* L., three potential invasive alien plants in Iran. To assess the *TAM* model's efficiency against conventional methods, we selected Bradford's model [10] for comparison. Experimental data on *A. psilostachya*, *C. acutum*, *B. pilosa* germination were applied to both *TAM* and Bradford's models, and then model fit and parameters were compared. Here, we: 1) explain the algorithm used to develop the new hydrothermal time calculation, 2) discuss its advantages and applicability through a comparison to Bradford's model, and 3) demonstrate the germination behavior of *A. psilostachya*, *C. acutum*, and *B. pilosa* under interactive temperatures and water potentials using the developed *TAM*.

2. Materials and methods

2.1. Model development

2.1.1. Calculating thermal time with sub-optimal temperatures

To determine the thermal time (TT_g) needed to achieve each germination fraction *(g)*, we employ the assumption of a right-angled triangle. In this triangular model, the base is computed as follows:

$$TTg_{(sub)} = (T - T_b) \times \quad t_g \tag{2}$$

where T represents the ambient temperature, and t_g denotes the time to reach the germination fraction (g). The height of the triangle corresponds to the accumulated value of $TT_{g(sub)}$, abbreviated as CTT_g, representing the cumulative thermal time required to reach the germination fraction at T. In this context, assuming a right-angled triangle, the hypotenuse connects the TT_g at *t=0* to CTT_g. The slope of this hypotenuse *(HS_sub)* serves as the determining parameter for calculating the CTT_g value at T relative to the CTT_g value at the optimum temperature *(T_o)*. If

T is closer to T_b, *HS_sub* is expected to be smaller. To address this, we utilize the following formula:

$$HS\_sub_{(T)} = HS\_sub \times \left(1 - \frac{(T_o - T)}{(T_o - T_b)}\right) \quad (3)$$

therefore, for temperatures further away from T_o, the *HS_sub* is smaller, resulting in a correspondingly smaller CTT_g. A key parameter reflecting the highest CTT_g is the maximum value of the cumulative germination fraction at T_o, abbreviated as G_m. Hence, we calculate CTT_g at T as follows:

$$CTTg_{(sub)} = HS\_sub_{(T)} \times \quad G_m \quad (4)$$

The area of the triangle for T on the sub-optimal side, abbreviated as AT_{Tsub}, is calculated as follows:

$$AT_{Tsub} = \left(\frac{1}{2}\right) \times TTg_{sub} \times CTTg_{(sub)} \quad (5)$$

2.1.2. Calculating thermal time with supra-optimal temperatures

On the supra-optimal side, TT_g is calculated using the following formula:

$$TT_{g(\sup)} = (T_c - T) \times t_g \quad (6)$$

The slope of the hypotenuse with supra-optimal temperatures (*HS_sup*) is calculated using Eq. 7:

$$HS\_\sup_T = HS\_\sup \times \left(1 - \frac{(T - T_o)}{(T_c - T_o)}\right) \quad (7)$$

therefore, CTT_g at supra-optimal temperatures is calculated as follows:

$$CTTg_{(\sup)} = HS\_\sup_{(T)} \times \quad G_m \quad (8)$$

the area of triangle for T on the supra-optimal side, abbreviated as AT_{Tsup} , is calculated as follows:

$$AT_{Tsup} = \left(\frac{1}{2}\right) \times TTg_{\sup} \times CTTg_{(\sup)} \quad (9)$$

2.1.3. Calculating Hydrotime (HT_g) to estimate the germination fraction

Right-angled triangles are employed to estimate HT_g for any germination fraction. For water potentials *(Ψ)* lower than Ψ_b, the base of the triangle is calculated as follows:

$$HT_g = |\Psi - \Psi_b| \times t_g \quad (10)$$

The height of the triangle is the cumulative hydro-time to reach the maximum germination fraction at Ψ, abbreviated as CHT_g. To estimate CHT_g, similar to thermal time calculations, a parameter of hypotenuse slope *(WS)* is multiplied by G_m. Therefore, the area of the triangle is obtained as follows:

$$AT_{(\Psi)} = \frac{1}{2} \quad \times WS \times G_m \times CHT_g \quad (11)$$

2.1.4. Hydrothermal time (HTT_g) calculation and prediction of the germination fraction

The hydrothermal time for a specific germination fraction (g) is given by the following equations for the sub-optimal and supra-optimal temperatures, respectively:

$$HTT_{g(sub)} = \frac{1}{t_g} \times AT_{Tsub} \times AT_{(\Psi)} \quad (12)$$

$$HTT_{g(\sup)} = \frac{1}{t_g} \times AT_{T\sup} \times AT_{(\Psi)}$$

We utilize $HTT_{g(sub)}$ and $HTT_{g(sup)}$ to calculate the base water potential for any fraction of the seed population ($\Psi_{b(g)}$) as follows:

$$\text{If } T_b < T < To, \Psi_{b(g)} = \Psi - (\theta_{HT} / HTT_{g(sub)}) \quad (13)$$

$$\text{If } T_o < T < Tc, \quad \Psi_{b(g)} = \Psi - (\theta_{HT} / HTT_{g(\sup)})$$

where θ_{HT} is the hydrothermal time coefficient [10].

The cumulative germination fraction (g) is predicted using the following equation:

$$\text{If } T_b < t < T_o, \quad g = (1 / (\sigma\sqrt{2\pi})) \times e^{\wedge}(-0.5) \times ((\Psi_{b(g)sub} - \mu)/\sigma) \quad (14)$$

$$\text{If } T_o < t < T_c, \quad g = (1 / (\sigma\sqrt{2\pi})) \times e^{\wedge}(-0.5) \times ((\Psi_{b(g)\sup} - \mu)/\sigma)$$

where μ is the mean Ψ_b, and σ is the standard deviation of Ψ_b.

2.2. Test species and data collection

In Iran, *A. psilostachya* is an invasive perennial species that significantly impacts the environment and the public health, particularly in the northern regions and along the western Caspian seashore [42]. While currently confined to roadsides and uncultivated land [1], its allergenic pollen increasingly poses an health risk [12]. *Cynanchum acutum*, also an invasive perennial species, exhibits a moderate potential for invasion in Iran [40]. It poses a significant challenge as a weed in orchards, especially in pistachio and vineyards, as well as sugarcane farms in the southwest of the country [22,25]. *Bidens pilosa* has also emerged as an invasive non-native species, particularly in central Iran in Fars, and has become problematic in orchards, and recent experiments have demonstrated its high potential for invasion in new habitats such as crop fields and prairies [29].

Seeds of *A. psilostachya* were collected from mature plants growing on roadsides in Bandar- Anzali (37.4639 *N*, 49.4799 *E*) on the west coast of the Caspian Sea in September 2020. Seeds of *C. acutum* were collected from Ahvaz (31.3183 *N*, 48.6706 *E*) in the southwest of Iran during October 2020. Dark yellow seeds were specifically selected for the experiment to ensure their phenological maturation stage. Seeds of *B. pilosa* were collected from orchards in Marvdasht (29.5243 *N*, 52.4824 *E*), Fars, Iran, where they have caused significant damage. In order to include some intraspecific genetic variation, seeds of each species were collected from each ten mother plants of three population, and then combines into a bulk sample, packed in paper bags and transferred to the laboratory for the experiment. After one month of storage, they were disinfected in 5% sodium hypochlorite for two minutes and then rinsed for three minutes [45]. Before commencing the experiment, Petri dishes with a width of 12 cm and Whatman filter papers (size 22) were autoclaved for two hours. Fifty seeds were carefully placed in each Petri dish for the germination test. The experiment followed a randomized complete design with a factorial arrangement of treatments. Factor one consisted of temperatures ranging from 5 to 40 °*C* (in increments of 5 °*C*) for *A. psilostachya*, from 10 to 50 °*C* (in increments of 10 °*C*) for *C. acutum*, and from 5 to 35 °*C* (in increments of 5 °*C*) for *B. pilosa*. Factor two consisted of moisture osmotic potentials of 0, -0.2, -0.4, and −0.6 MPa for *A. psilostachya*, and 0, -0.3, -0.6, -0.9, -1.2, and −1.5 MPa for *C. acutum*, and 0, -0.2, -0.4, -0.6. -0.8, and −1 MPa for *B. pilosa*. The germination test was replicated four times. All germination tests were conducted in darkness [14,32]. To prepare the osmotic potentials, we utilized polyethylene glycol (*PEG 6000*) based on the formula described in previous studies [24,26] as follows:

$$\Psi_S = -(1.8\times10^{-2})\,C - (1.8\times10^{-4})\,C^2 + (2.67\times10^{-4})\,CT + (8.39\times10^{-7})\,C^2T \quad (15)$$

where Ψ_s is the required osmotic potential (*Bar*), C is the *PEG* concentration (*g/L*), and T is the temperature (°*C*). We verified the osmotic potential using an osmometer (Gonotec® Osmomat® Freezing Point

Osmometer Model 3000) to ensure the accuracy of the provided water potentials. Five mL of the solution was added to the Petri dishes according to the experimental design. The Petri dishes were then sealed with parafilm and placed in the germinator. Germination was monitored and counted every 24 h for 14 days. To ensure consistency, eight germinators were set up simultaneously at the experimental temperatures.

2.3. Statistical analysis

The distributions of germination data were examined using a histogram plot and a normal quantile plot. Due to higher levels of dormancy in *A. psilostachya* and *C. acutum*, their germination fraction did not exceed 70%, and there were frequent instances when no germination was observed. As a result, pronounced deviations from normality were noted in all studied species, with *A. psilostachya* and *C. acutum* exhibiting higher levels than *B. pilosa*. Model development and fitting were conducted using R-Studio [37].

We utilized the *truncnorm* package to handle truncated normal distributions, employing the *ptruncnorm* function to generate values from a truncated normal distribution. This process was specifically applied to variables $\Psi_{b(g)}sub$ and $\Psi_{b(g)}sup$ at both sub-optimal and supra-optimal temperatures. A linear regression model was then fitted using the *lm* function. The response variable was the observed germination fraction, and the predictor variable was the truncated normal distribution (predicted germination fraction). Model evaluation included obtaining summary statistics of the fitted linear regression model, such as coefficients, standard errors, t-values, and p-values, using the summary function. Performance metrics like *RMSE*, R^2, and Residual Standard Error (*rse*) were calculated. To display the cardinal temperatures and base water potentials, we utilized a 4-parameter log-logistic model [11] from the drc package [35]. This model was used to describe the cumulative germination fraction over time for various combinations of experimental temperature and water potential. We calculated the time required to reach any percentile of the germination fraction, which was then normalized to the observed G_m for each species. To ensure a thorough representation of the data, we employed germination rates corresponding to various percentiles. This approach enables us to draw conclusions across lower, middle, and upper percentiles of germinations. In establishing germination rates for each species, we calculated the reciprocal of the time to reach any germination fraction, considering the experimental temperature and moisture combinations. Subsequently, we applied a two-segment function to describe the relationship between germination rates and experimental temperature, and a linear model to depict the relationship between germination rates and different experimental water potentials [9]. We applied *TAM* and Bradford's model to the datasets of the three study species conducting a comparative analysis to assess their respective fits. The methods for model comparison involved evaluating parameter estimates, and key statistical measures including sum-of-squares, the number of parameters, Akaike's Information Criterion corrected (*AICc*), and an F test.

3. Results

3.1. Thermal time calculation with TAM

Fig. 1 illustrates that both *ATTsub* and *ATTsup* values can be effectively represented using right-angled triangles at each temperature. On both sub-optimal and supra-optimal sides, multiple right-angled triangles with varying hypotenuse slopes exist. For sub-optimal temperatures, as the temperature approaches T_o, *HS_sub*, and consequently $G_{(T)}$, increase, resulting in the formation of larger triangles. The largest triangle area occurs at the optimum temperature, with a height corresponding to G_m and estimated values of 17293, 4869, and 4628 °C hours for *A. psilostachya*, *C. acutum*, and *B. pilosa*, respectively (Fig. 1).The difference between T and T_o significantly influences the triangle's size at each temperature through two factors: 1) the distance of T from T_b, 2) the distance of T from T_o.

On the supra-optimal side, as T increases towards T_c, *HS_sup* decreases, leading to a decrease in $G_{(T)}$. Consequently, smaller triangles form as T approaches T_c. Notably, biologically, the difference between T_o - T_b is larger than T_c - T_o, resulting in a greater number of triangles on the sub-optimal side compared to the supra-optimal side. By applying this approach, we computed the thermal time for germination fractions with both sub-optimal and supra-optimal temperatures. They are illustrated in Fig. 1 for *A. psilostachya*, *C. acutum*, and *B. pilosa*.

3.2. Hydrotime calculation with TAM

We demonstrate that the hydro time calculation, derived from Eq. (11) and illustrated in Fig. 2, corresponds to the cumulative area of triangles over time associated with different water potentials. The cumulative hydro time is represented by the total area covered by these triangles (Fig. 2). The coefficient $G_{(\Psi)}$ exhibits a lower value under drier conditions, resulting in smaller triangles at more negative water potentials. Conversely, when greater moisture is available (resulting in less negative water potentials), the coefficient $G_{(\Psi)}$ increases, subsequently leading to the increase of and the formation of larger triangles. This, in turn, results in higher calculated hydro time values.

Our findings underscore the significant reliance of HT_g calculation on the values of Ψ_b and $G_{(\Psi)}$. This dependence is evident from our computation of HT_g for *A. psilostachya*, *C. acutum*, and *B. pilosa* (Fig. 2), in which the area of triangles increase as the water potential shifts towards zero.

3.3. Hydrothermal time calculation with TAM

By multiplying $AT_{(T)}$ by $AT_{(\Psi)}$ and then dividing by tg, we derived HTT_g, representing hydrothermal time triangles. These triangles, depicted in Fig. 3, exhibit a high degree of sensitivity to fluctuations in both temperature (T) and moisture (Ψ). In addition to HTT_g triangles, we simultaneously demonstrate the cumulative germination fractions corresponding to each HTT_g estimation. As shown, HTT_g and cumulative germination fractions are highly correlated, and for some T and Ψ combinations, the R^2 values are as high as 0.99. Changes in the area of HTT_g triangles result in corresponding synchronous changes in cumulative germination fractions. This demonstrates the effectiveness of the *TAM* approach in calculating HTT_g values, both in terms of methodology for considering the T status in relation to the cardinal temperatures and in terms of the Ψ value in relation to the Ψ_b.

3.4. TAM model performance

We applied model (14) using HTT_g values as input variables to predict germination fractions over time. The model was effectively fitted to the germination data of *A. psilostachya* (R^2=0.96, *RMSE*=0.03), *C. acutum* (R^2=0.97, *RMSE*=0.03), and *B. pilosa* (R^2=0.98, *RMSE*=0.05) (Table 1).

Using *TAM*, we determined base temperatures (T_b) for *A. psilostachya*, *C. acutum*, and *B. pilosa* as 0.19 °*C*, 14.57 °*C*, and 5.76 °*C*, and the optimal temperatures at 25.1°*C*, 39.9 °*C*, and 29.8 °*C*, respectively. Additionally, the ceiling temperatures were found to be 46.74 °*C*, 53 °*C*, and 41°*C* for *A. psilostachya*, *C. acutum*, and *B. pilosa*, respectively (Table 1). In Fig. 4, we depict the germination rates plotted against experimental temperatures. The intersections of the fitted lines with the temperature axis indicate the values for T_b and T_c. The optimum temperature is also identified by the temperature corresponding to the highest predicted germination rates. Both T_b and T_c parameters vary with different germination percentages, upon which the germination rates were calculated, as well as the water potential at which the parameters were estimated. The T_b values for *A. psilostachya*, *C. acutum*, and *B. pilosa* were estimated to be 0.18 (±2.95), 15 (±2.3), and 5.8 (±2.6), and the T_o values as 25.5 (±0.6), 39 (±0.71), and 29 (±0.41),

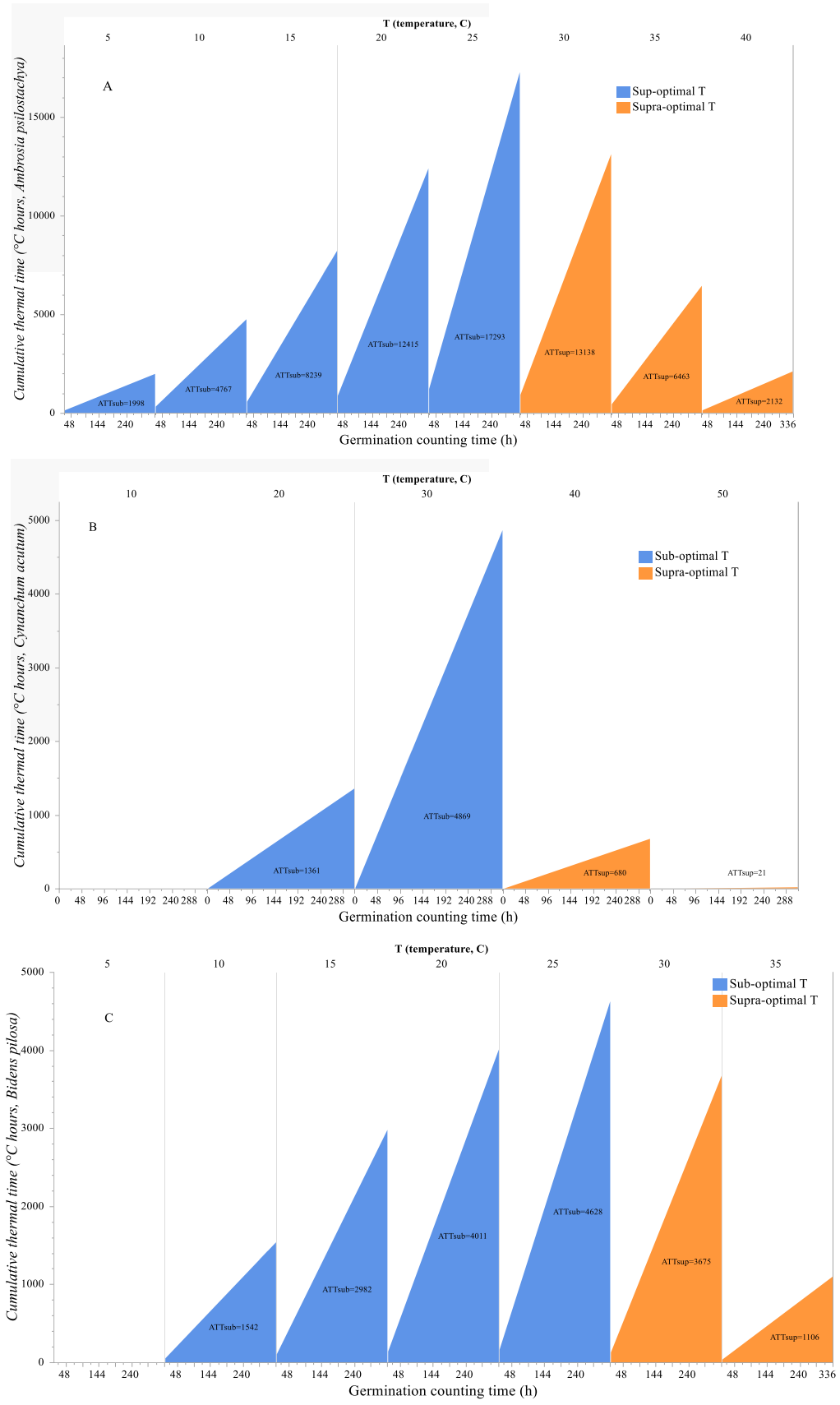

Fig. 1. Thermal time right-angled triangles are depicted with the sub-optimal and supra-optimal temperatures for *A. psilostachya* (A), *C. acutum* (B), *and B. pilosa* (C) germination using *TAM*. The area of each triangle represents cumulative thermal time along with the corresponding temperature.

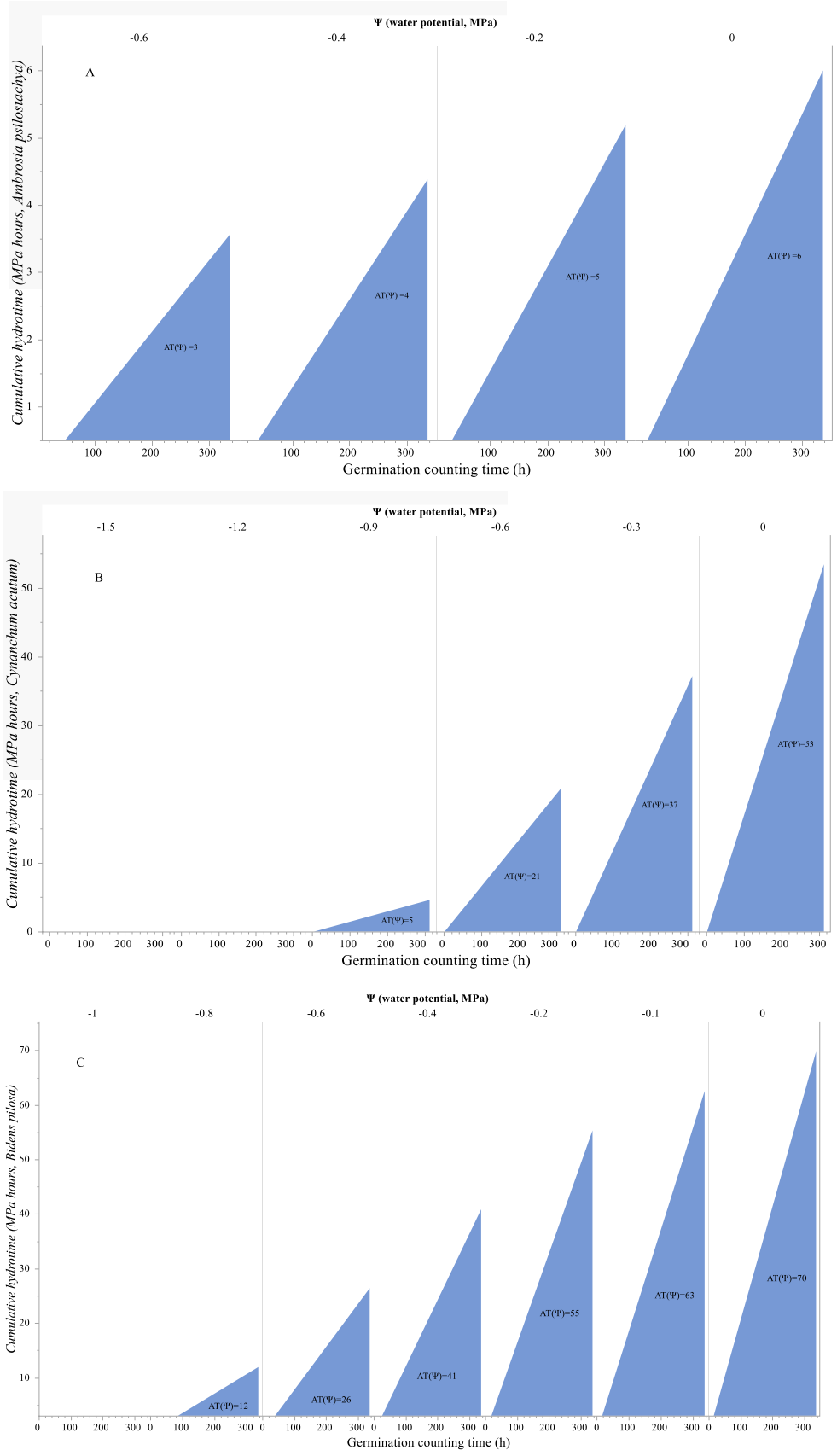

Fig. 2. Hydro time right-angled triangles are depicted with the sub-optimal and supra-optimal temperatures for *A. psilostachya* (A), *C. acutum* (B), *and B. pilosa* (C) germination using *TAM*. The area of each triangle represents cumulative hydro time along with the corresponding water potential.

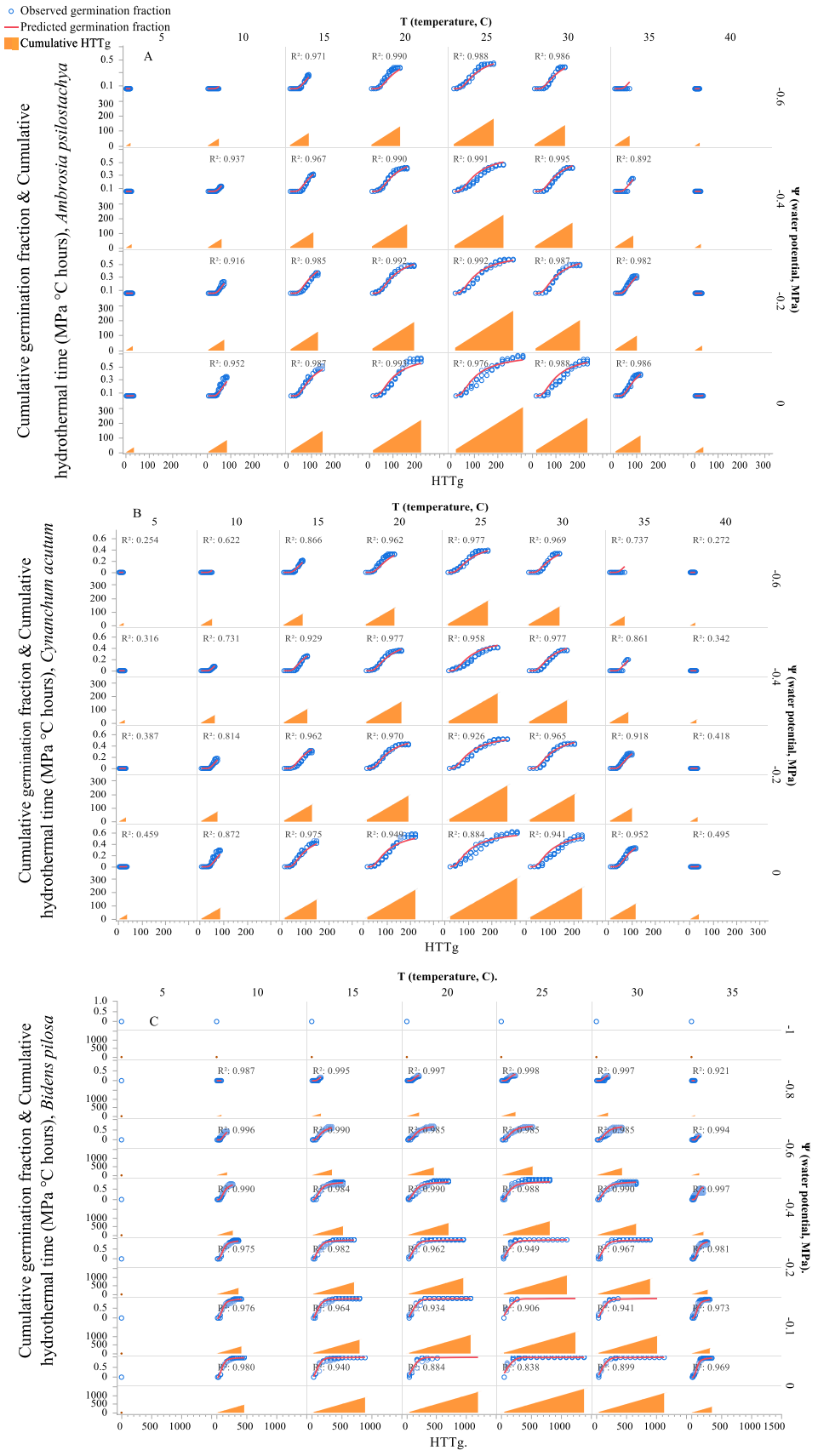

Fig. 3. Cumulative germination fractions of *A. psilostachya* (A), *C. acutum* (B), *and B. pilosa* (C) seeds vs. cumulative hydrothermal time depicted as the right-angled triangles in orange with various combinations of temperatures and water potentials. The area of each triangle corresponds to the accumulated hydrothermal time for the corresponding germination fraction.

Table 1
Parameter estimates for the germination of *A. psilostachya*, *C. acutum,* and *B. pilosa* as affected by temperature and moisture obtained using the *TAM* and Bradford model.

Parameter estimates	Plant species					
	A. psilostachya		*C. acutum*		*B. pilosa*	
	TAM	*Bradford*	*TAM*	*Bradford*	*TAM*	*Bradford*
T_b (°C)	0.19	0.23	14.57	9	5.7	3.87
T_o (°C)	25.1	27.8	39.9	31	29.9	27.8
T_c (°C)	46.74	-	53	-	41	-
ψ_b (MPa)	-1.42	-0.93	-0.97	-0.94	-0.96	-0.71
$\sigma_{(\Psi)}$	2.95	0.89	2.14	0.36	0.45	0.22
G_m	0.70	-	0.63	-	1	-
HS-sub	2.92	-	2.03	-	1.7	-
HS-sup	8.55	-	0.55	-	2.9	-
θ_{HT}	314.8	4768	137.6	1578	89	383
WA	0.03	-	0.55	-	0.430	-
R^2	0.96	0.95	0.97	0.87	0.98	0.97
RMSE	0.03	0.04	0.03	0.06	0.04	0.07

respectively. The T_c values for *A. psilostachya*, *C. acutum*, and *B. pilosa* were estimated to be 47 (±5), 52 (±4), and 42 (±5), respectively. Therefore, the mean T_b, T_o, and T_c estimated values are consistent with those determined by *TAM*.

In Fig. 5, we present the germination rates for each species plotted against experimental water potentials at various temperatures. The point where the fitted line intersects with the water potential axis represents the Ψ_b value for each species. As depicted, Ψ_b varies with different germination percentages, upon which the germination rates are calculated, as well as the temperatures over which the relationship between germination rates and water potentials is assessed. The Ψ_b values for *A. psilostachya*, *C. acutum*, and *B. pilosa* were estimated to be -1.5 (±0.8), -1.07 (±0.7), and 0.98 (±0.8), respectively, indicating that the mean Ψ_b values are consistent with those estimated by *TAM*. The mean base water potential estimated by *TAM* is -1.48 for *A. psilostachya*, -0.98 for *C. acutum*, and -0.97 for *B. pilosa*.

3.5. A comparison of TAM and the Bradford's model

We applied Bradford's hydrothermal model to the data of *A. psilostachya*, *C. acutum*, and *B. pilosa* to compare *TAM*'s predictions with a widely used approach for estimating hydrothermal time germination. Table 1 presents both model fit metrics and parameter estimates for Bradford's model and *TAM*. Bradford's model yielded R^2 values of 0.94 and *RMSE* of 0.04 for *A. psilostachya*, R^2 of 0.86 and *RMSE* of 0.09 for *C. acutum*, and R^2 of 0.95 and *RMSE* of 0.07 for *B. pilosa* (Fig. 6).

For *A. psilostachya*, the parameter estimates were: T_b=0, T_o=28.8, θ_{HT}=4768, Ψ_{b50}=-0.94, and σ=0.89, for *C. acutum* T_b=9, T_o=31, θ_{HT}=1578, Ψ_{b50}=-0.94, and σ=0.36, and for *B. pilosa* T_b=3.4, T_o=28, θ_{HT}=481, Ψ_{b50}=-0.73, and σ=0.22. Fig. 7 illustrates the fit of both *TAM* and Bradford models to the observed cumulative germination fractions. While both models fit well with the cumulative germination fractions, it is evident that *TAM* provides better fits over temperatures and moisture levels beyond the optimal values. Additionally, we found a significantly better fit of *TAM* to the *C. acutum* data compared to the Bradford model. *TAM* yields parameter estimates that are more biologically logical and justifiable when compared to the germination behavior of the species. Furthermore, *TAM* generates biologically more meaningful parameters, offering deeper insight into the species' germination as affected by temperature and moisture. The results of the model comparison suggest that *TAM* is a more suitable model than Bradford's model for explaining germination fractions over time for the three study species (Table 2). Two distinct evaluation approaches, *AICc* and the F-test, consistently support this conclusion. *TAM* exhibited a significantly lower *AICc* than Bradford's model, suggesting a higher likelihood of being the correct model. The F-test further confirmed this preference for *TAM*, demonstrating a significant improvement in model fit compared to Bradford's model.

The clear disparities observed in *AICc* values, and the model fit improvements indicated by the F-test across all three species consistently support the recommended use of *TAM* over the Bradford's model, emphasizing its reliability in predicting germination fractions.

4. Discussion

4.1. Advantages of TAM over previous approaches

4.1.1. Sub-optimal side enhancement

In comparison to previous methods, which calculate TT_g by subtracting the base temperature (T_b) from the current temperature (T) and then multiplying the result by time [2], the *TAM* model employs a similar approach but with a crucial modification. In *TAM*, cumulative germination fraction corresponding to the given temperature, i.e., $G_{(T)}$ is incorporated into the calculation. This adjustment recognizes that when seeds germinate at temperatures considerably lower than the optimum, a one-degree rise in temperature has a less pronounced effect on promoting germination compared to a one-degree rise in temperature closer to the optimal range. To illustrate this, let's consider two species, denoted as species *A* and species *B*, each with the same T_b value of 4 °C and varying optimal temperatures (T_o) of 20 °C and 25 °C, respectively. In traditional methods, the thermal time at a T of 10 °C would be calculated exactly the same as (10−4) × the time unit, while *TAM* considers additional parameters such as the distance between T and T_o, and the $G_{(T)}$ that occurs with T. Therefore, to achieve this, *TAM* needs final cumulative germination fraction (G_m) that occurs with ultimate germination counting time at T_o, and a parameter of *HS_sub*. Thus, to calculate TT_g, (10−4) should be multiplied by $(1-((T-T_b)/(T_o-T_b))) \times G_m \times HS\_sub$. We have shown through calculating $TT_g(sub)$ for three study species that *TAM* possessed a more informative and accurate approach for $TT_g(sub)$ calculation compared to previous models.

4.1.2. Supra-optimal side refinement

When it comes to calculating TT_g on the supra-optimal side, previous methodologies demonstrate even greater limitations compared to their sub-optimal counterparts. In certain approaches, *TT* is added directly to the ceiling temperature (T_c), employing the same methodology as used for sub-optimal conditions [15]. Slightly improved methods halt the calculation at the optimum temperature, failing to extend beyond it and persistently subtracting T_b from T_o for any temperature beyond T_o. However, *TAM* takes a significantly different and more nuanced approach, considering the specific germination fraction at each temperature $G_{(T)}$ as a pivotal factor. As T approaches T_c, $G_{(T)}$ tends to decrease. In *TAM*, this phenomenon is meticulously addressed by introducing the concept of hypotenuse slope, which is then multiplied by the G_m to estimate germination rate at the corresponding temperature. Also, *TAM* considers the distance of T to T_c, and the distance of T_o to T_c. This dynamic adjustment ensures that as temperatures move closer to T_c, smaller triangles are formed, consequently resulting in lower TT_g calculations. This insight is rooted in the hypothesis that seeds germinating at temperatures around T_c do not possess the same capacity to accumulate thermal time as seeds germinating at temperatures around the optimal range. The physiological status of seeds germinating near critical temperatures, such as those approaching T_c, inhibits their responsiveness to ambient temperatures [47]. The interactions among *GA* metabolism and *GID1-type* receptor signaling in crucial seed compartments, along with the spatiotemporal patterns, govern tissue connections and the timing of germination in reaction to surrounding environmental signals. Gibberellins play a vital role in seed temperature reactions, and they engage with other hormonal pathways amid thermos-inhibition. Allelochemicals like myrigalone A obstruct seed germination through targeted disruption of *GA* metabolism and signaling pathways [44].

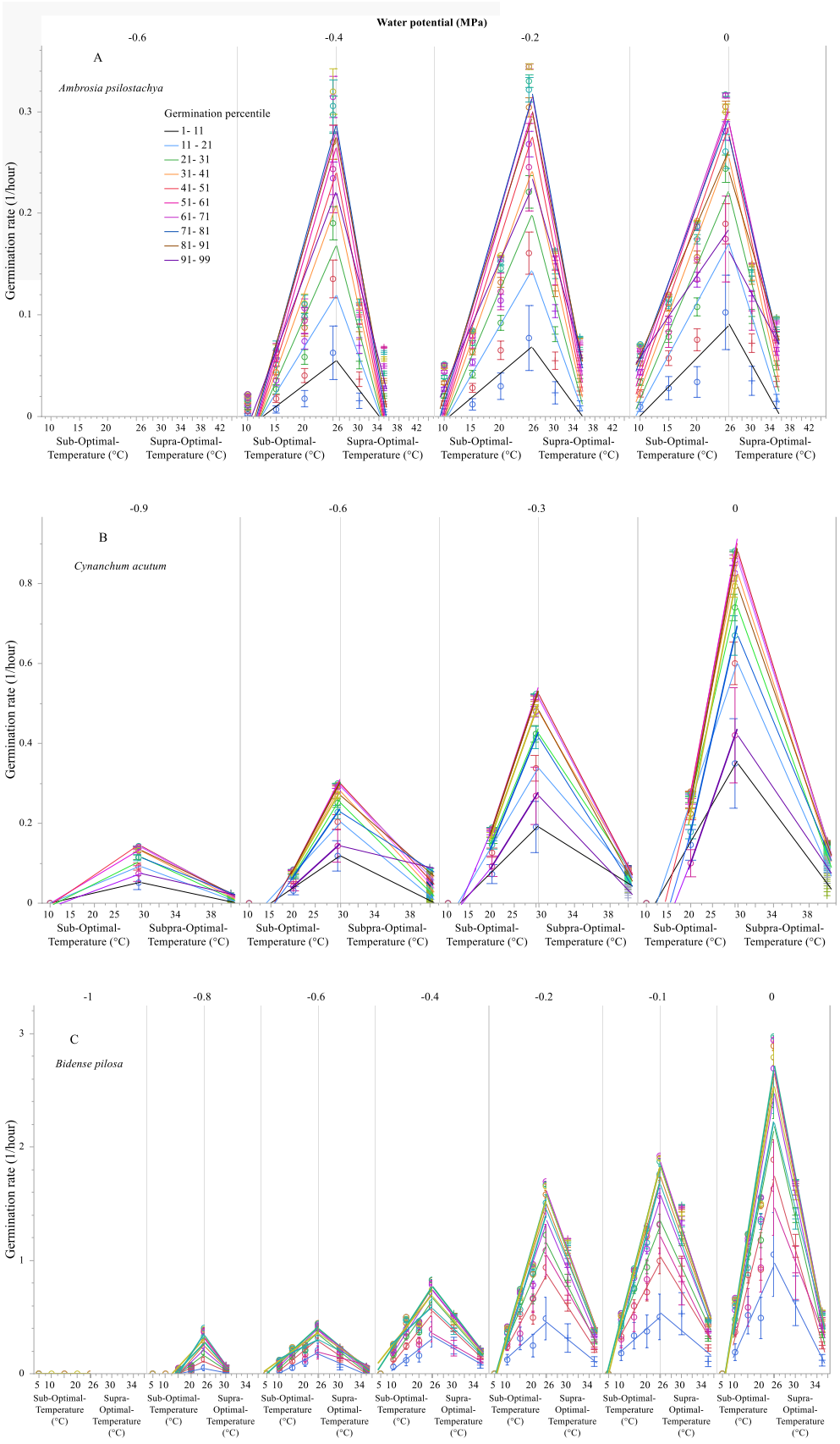

Fig. 4. Relationship between the germination rates and experimental temperatures for various water potentials for (A) *A. psilostachya*, (B) *C. acutum*, and (C) *B. pilosa*. The error bars are standard deviations of mean germination rates over germination decile.

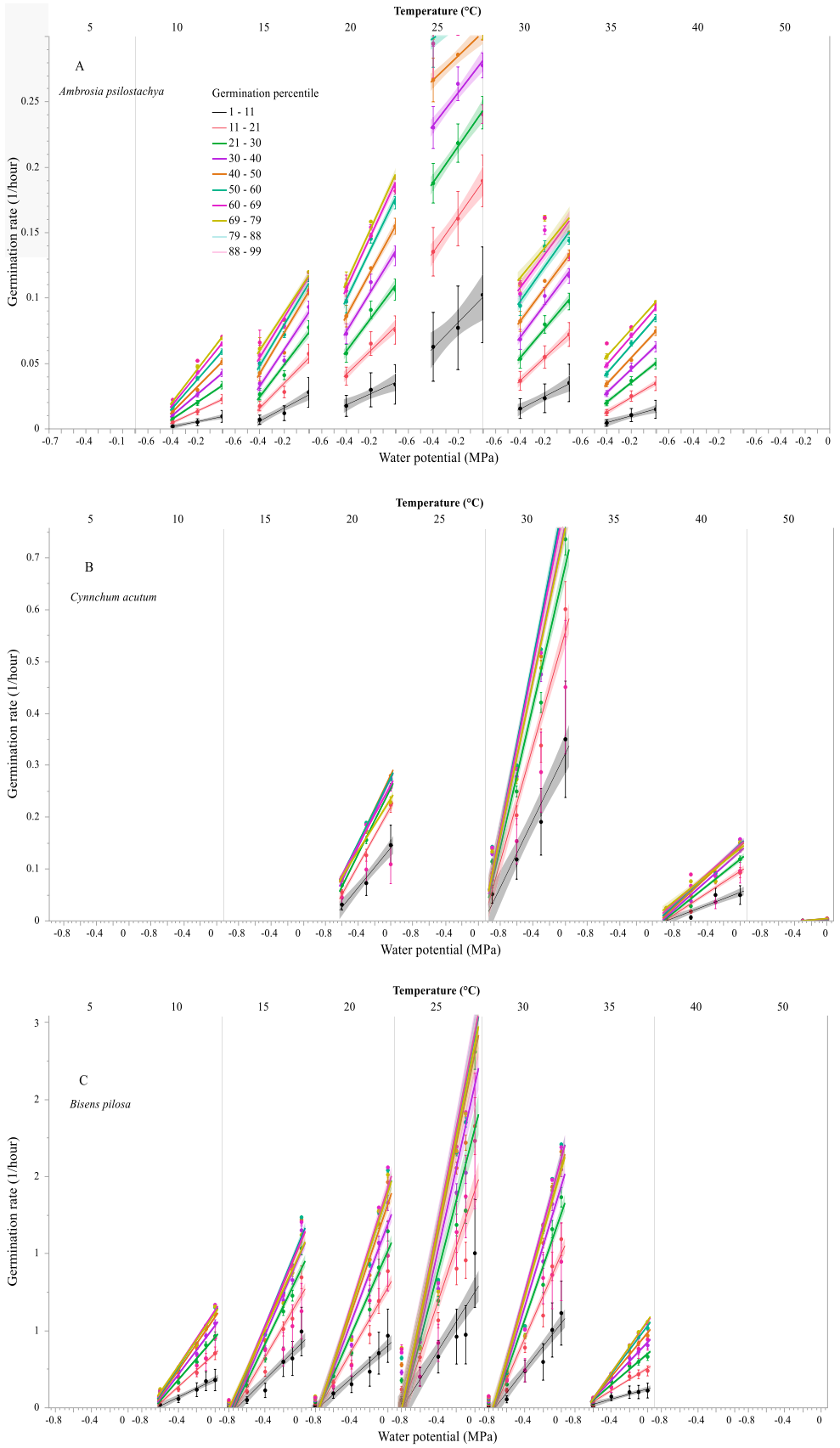

Fig. 5. Relationship between the germination rates and experimental water potentials for various temperatures for (A) *A. psilostachya*, (B) *C. acutum*, and (C) *B. pilosa*. The error bars are standard deviations of mean germination rates over germination decile.

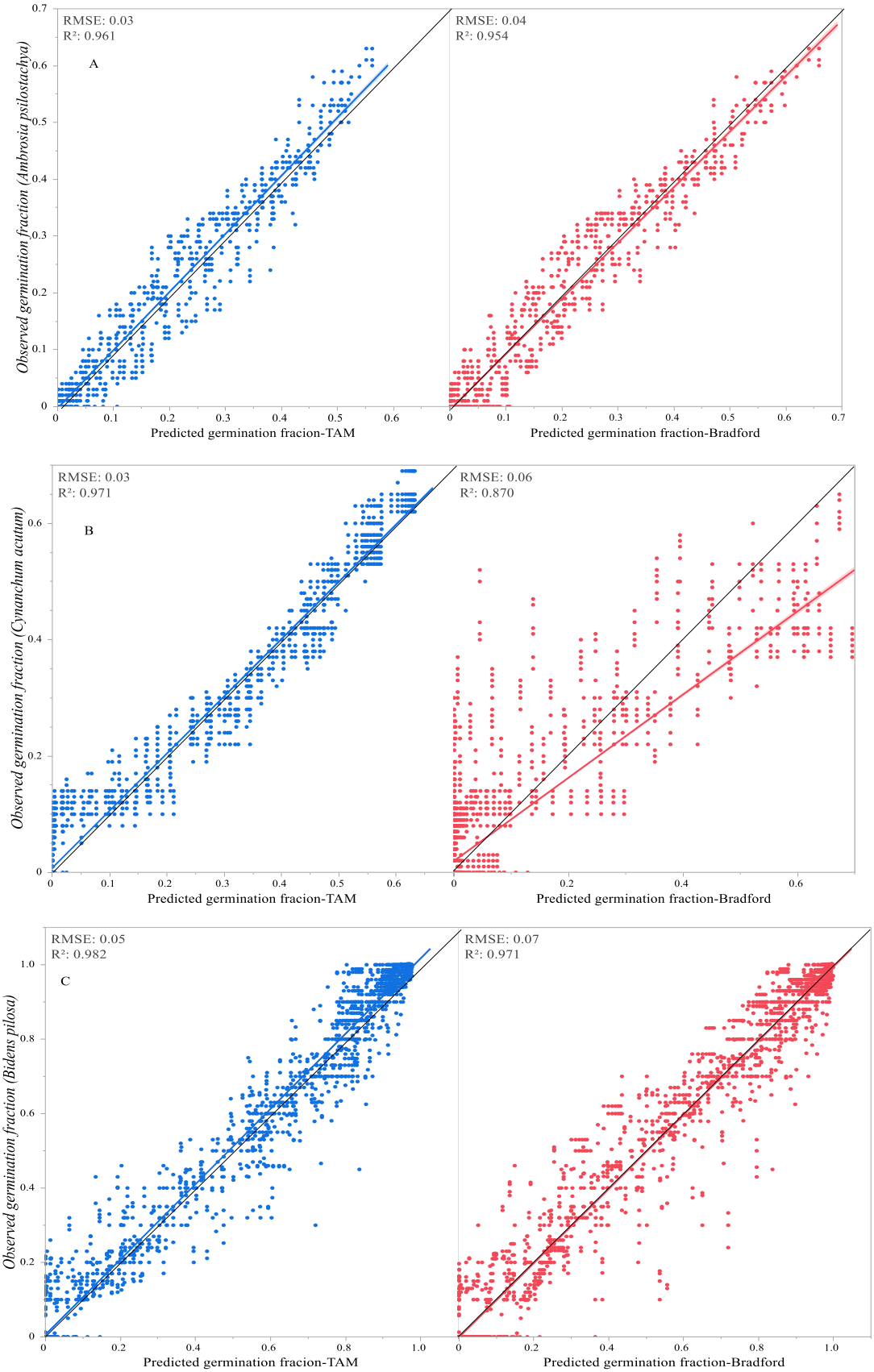

Fig. 6. Observed and predicted germination of *A. psilostachya* (A), *C. acutum* (B), *and B. pilosa* (C) are presented using the *TAM* and Bradford's model. Model fit indices, along with a dashed one-to-one line, are provided to assess and compare the model fits.

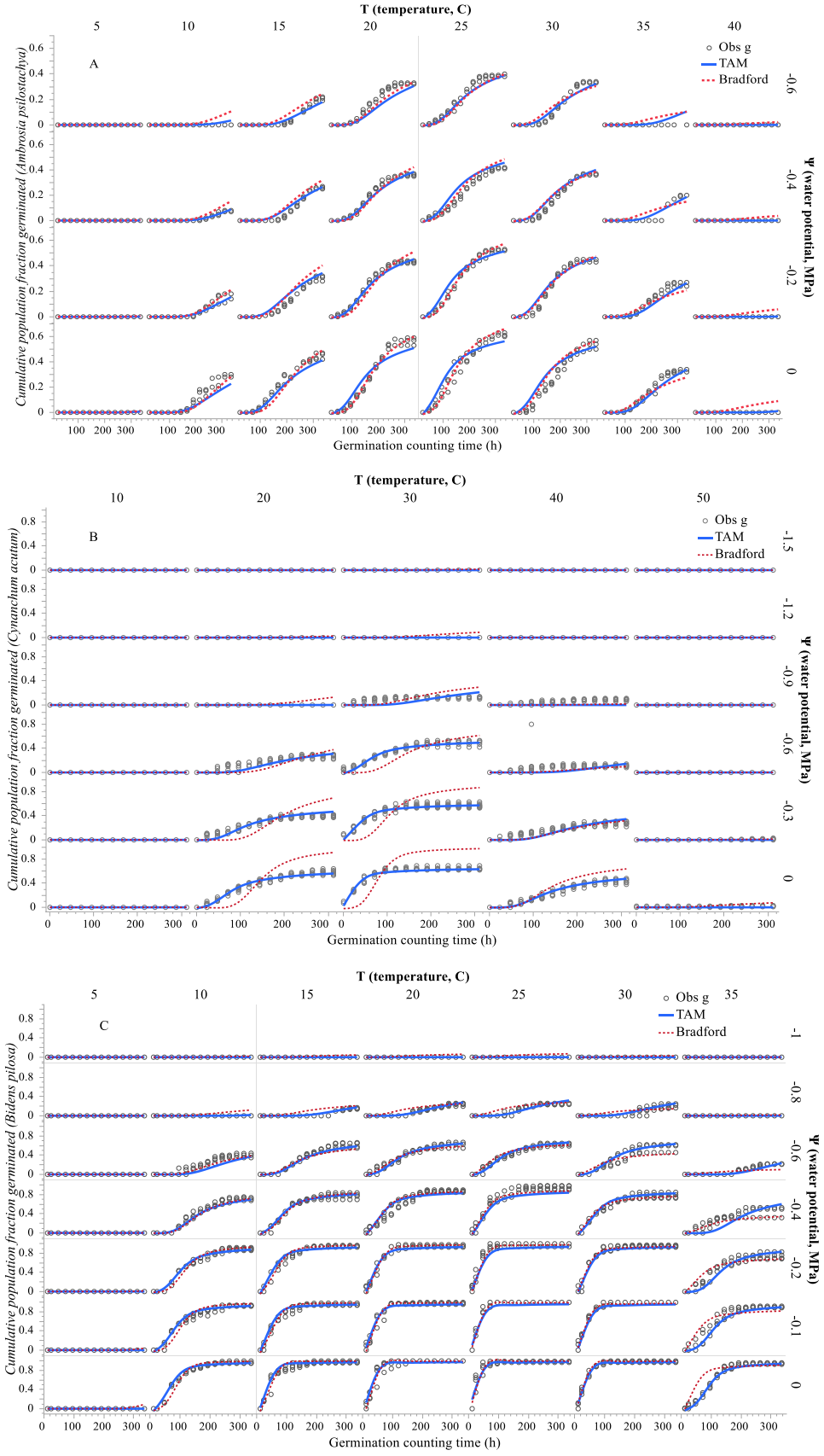

Fig. 7. The cumulative germination of *A. psilostachya* (A), *C. acutum* (B), *and B. pilosa* (C) over germination counting time displayed across a range of experimental temperatures and various water potentials. The predicted cumulative germination fractions by *TAM* are shown in solid blue lines, and by Bradford's model in dashed red lines, while the observed cumulative germination fractions are represented by gray circles.

Table 2
Comparison of *TAM* model with Bradford's hydrothermal model for *A. psilostachya*, *C. acutum* and *B. pilosa* data.

Model	*A. psilostachy*		*C. acutum*		*B. pilosa*	
	TAM	Bradford	TAM	Bradford	TAM	Bradford
Sum-of-squares	3.68	3.92	1.48	3.92	9	13.6
Number of data points	2688	2688	2520	2520	2744	2
Number of parameters	10	6	10	6	10	6
AICc	-17534	-17374	-19971	-17381	-1700	-1579
Probability (%)	>99.99	<0.01	>99.99	<0.01	>99.99	<0.01
Difference in AICc	160	-	2584	-	1206.13	-
Ratio (F)	43.3	-	1095	-	374	-
P value	<0.0001	-	<0.0001	-	<0.0001	-

4.1.3. Hydro time calculation advancement

Previous methodologies have incorporated modification coefficients to adjust the base water potentials beyond optimal temperatures [2]. These approaches propose a constant value for Ψ_b at sub-optimal temperatures and posit that it starts increasing as temperatures approach the ceiling temperature. In *TAM*, hydro time is conceptualized as being exclusively determined by differently sized right-angled triangles, each representing a unique water potential, regardless of temperature variations. In this model, the base of the triangle is established as $(\Psi-\Psi_b)\times t_g$, while the germination fraction corresponding to the specific water potential and t_g *i.e.* $G_{(\Psi)}$ is represented by the triangle's height. As conditions become drier (more negative Ψ) leading to lower $G_{(\Psi)}$ values, smaller triangles characterized by reduced heights emerge. Calculating the height necessitates the multiplication of the hypotenuse slope by G_m, which is observed at a water potential of zero. This approach mirrors the methodology employed for TT_g calculation. Consequently, seeds germinating under drier conditions exhibit reduced responsiveness to environmental changes, including moisture increase. In contrast, seeds with ample moisture experience heightened enzymatic activities, enhancing their capacity to respond to fluctuations in ambient moisture [30]. Seeds contain essential growth substrates within embryos, endosperm, or perisperm, including polysaccharides, proteins, triglycerides, phytic acid, and salts. These substrates need to be hydrolyzed from their stored forms. The metabolic processes responsible for hydrolysis, synthesis, and energy production operate at a slower pace under water stress. However, when sufficient moisture is available, respiratory activity increases, leading to higher germination catalyst levels. This, in turn, facilitates hydrolysis and enzyme activation [27].

4.1.4. Hydrothermal time calculation refinement

In the pursuit of HTT_g determination, *TAM* seamlessly marries the calculated hydro and thermal units by incorporating the element of time. This unique approach accounts for the dynamic interplay between temperature and moisture in the germination process. For instance, if seeds germinate near the optimal temperature but are exposed to a water potential close to the threshold of the base value, the HTT_g triangle's expansion becomes constrained by moisture limitations. Conversely, when the scenario is reversed, the size of the HTT_g triangle is restricted by the temperature factor. Thus, *TAM* adeptly captures and quantifies the intricate interdependency of temperature and moisture on germination. Within the framework of *TAM*, germination fraction at each T and ψ is an important determining parameter that enables the model to consider the level of germination or dormancy of a species at the time of germination testing. Therefore, if the final cumulative germination with T_o is low because of seed dormancy or any cause of lack of germinability, it's effect is involved in germination prediction.

4.2. Using TAM to fit germination data of A. psilostachya, C. acutum, and B. pilosa

Our approach proved highly successful in fitting the germination data of the three plant species. Through this application, we obtained robust estimates for the hydrothermal time parameters governing their germination dynamics. *Ambrosia psilostachya*, an invasive species to northern Iran, predominantly thrives in regions characterized by elevated precipitation levels. Consequently, its germination process is less susceptible to substantial fluctuations in soil moisture. Since its initial record in Iran [42], this species has proliferated across diverse habitats within the Gilan province along the western coastal perimeter of the Caspian Sea. Additionally, recent records indicate its presence in the Mazandaran province, extending along the eastern Caspian coastline with lower precipitation and less moistened soils [38]. Projections further anticipate its expansion and establishment into broader territories featuring reduced precipitation levels across the northwest and western sectors of Iran (Oveisi et al., 2023). Our forward-looking assessment of *A. psilostachya*'s germination response to temperature and moisture, coupled with the broad spectrum of temperature and moisture conditions anticipated for its germination, harmonizes seamlessly with existing projections. This alignment bolsters the notion of *A. psilostachya*'s forthcoming expansion, affirming the likelihood of its continued spread and impact.

Cynanchum acutum shows an increased sensitivity to fluctuations in water potential. Even when exposed to a relatively moderate water potential of −0.9 MPa, a significant decrease in cumulative germination fraction becomes apparent. This impact is not limited to altering the range of temperatures suitable for germination, but it also affects the pace of germination over time. Notably, despite its capability to germinate across a wide range of temperatures (with a T_c estimate of $53^{\circ}C$), this species is anticipated to expand its distribution to encompass the extensive warm climate regions of Iran in irrigated plant production systems where water is not a limiting factor. Currently, *C. acutum* presents a significant challenge within vineyards, and pistachio orchards in Takestan, Yazd and Kerman (Iran), which are located in arid regions [20, 39]. Furthermore, this species causes issues in sugarcane farms situated in the southwestern region of Iran, characterized by hot weather with temperatures above $50^{\circ}C$ in mid-summer [22]. As a result, its proliferation spans a diverse range of climates and agricultural settings. Notably, this species is projected to cause increasing impact under climate change, as it has demonstrated robust resistance to elevated temperatures [4].

Bidens pilosa recently became widespread in central Iran, particularly in Fars, mainly infesting orchards. High seed production [13] coupled with special barbs that make them highly dispersible through ectozoochory [33] are expected to favor its rapid population build up and expansive spread. Field experiments also demonstrated the high ability of *B. pilosa* in infesting crop fields such as legumes [46]. Using our *TAM* model we have shown that the range of temperature germination of this specie is very wide, and larger than for *A. psilostachya* and *C. acutum*. Also, the G_m value is near to one showing high germination potential of this species and low dormancy. This crucial information asks for appropriate management decisions.

4.3. Why does TAM outperform Bradford's model?

Bradford's model fitted well to data of *A. psilostachya* and *B. pilosa*, but less for *C. acutum* (Fig. 7). The parameter estimates did not

biologically align with the observed germination behaviors of the study plant species, with issues noted in the estimation of T_b and Ψ_b. When comparing the data structure, we find *C. acutum* germinated less uniform and with many zero records with time intervals. The final germination fraction of this species was 0.63 indicating levels of dormancy, while *A. psilostachya* and *B. pilosa* germinated more uniformly and for *B. pilosa* the final cumulative germination fraction of one was obtained. Thus, *TAM* could give a better prediction with data that have higher deviance from the normal distribution and show non-uniform germination over time.

5. Conclusion

We advocate that the *TAM* approach has the potential for a broader application in estimating thermal time, hydro time, and accordingly hydrothermal time for predicting germination fraction within a seed population. *TAM* possesses more informative parameters to highlight aspects of germination through the population, and considers crucial factors such as germination-dormancy or the general germinability within a population represented by the cumulative germination fraction at optimal T and ψ. *TAM* accentuates on the range between T_b and T_c, in which germination happens, and the position that T has in relation to T_b, T_o, and T_c and that ψ has in relation to ψ_b. The accurate performance of *TAM* asserts for the applicability of its approach for various other phenological growth stages. This is supported by the similarity between the *GDD* (Growing Degree Day) calculation for plant growth and the method employed in germination *TT* calculation [49]. However, we recognize that substantial additional research is imperative to validate and substantiate the extended utility of the *TAM* approach. This future exploration will not only shed light on the broader applicability of *TAM,* but also assess its potential to enhance the precision of plant growth predictions and in turn its potential for population build-up and spread.

Author contributions

Mostafa Oveisi and **Heinz Müller-Schärer** conceptualized the experiment. **Mostafa Oveisi** and **Hassan Alizadeh** designed and supervised the experiments. **Sassan A. Lorestani, Aboozar Esmaili**, and **Nasrin Sadeghnejad** performed the experiments and measurements. **Mostafa Oveisi** conducted data analysis and model development. **Mostafa Oveisi** and **Heinz Müller-Schärer** wrote the manuscript, and **Jose L. Gonzalez-Andujar** and **Ramin Piri** revised it.

Declaration of Competing Interest

The authors declare that they have no known competing financial interests or personal relationships that could have appeared to influence the work reported in this paper.

Data availability

Data will be made available on request.

Acknowledgements

This research was funded by the University of Tehran.

References

[1] Almasi S., Oveisi M., Tokasi S., M.-S.H., 2021. Environmental factors determining the shoot density of Ambrosia psilostachya, an invasive alien perennial species in northern Iran. Proc. Invasive Plants Work. Gr. EWRS Work. "Our Path After Covid-19," Palic, Serbia, 24.

[2] V. Alvarado, K.J. Bradford, Hydrothermal time analysis of seed dormancy in true (botanical) potato seeds, Seed Sci. Res. (2005) 15, https://doi.org/10.1079/ssr2005198.

[3] V. Alvarado, K.J. Bradford, A hydrothermal time model explains the cardinal temperatures for seed germination, Plant, Cell Environ. (2002) 25, https://doi.org/10.1046/j.1365-3040.2002.00894.x.

[4] B. Ar, G. Tuttu, D. Gülçin, A.U. Özcan, E. Kara, M. Sürmen, K. Çiçek, J. Velázquez, Response of an invasive plant species (Cynanchum acutum L.) to changing climate conditions and its impact on agricultural, Landsc. Land (2022) 11, https://doi.org/10.3390/land11091438.

[5] H. Balouchi, V. Soltani Khankahdani, A. Moradi, M. Gholamhoseini, R. Piri, S. Z. Heydari, B. Dedicova, Seed fatty acid changes germination response to temperature and water potentials in six sesame (Sesamum indicum L.) cultivars: estimating the cardinal temperatures, Agriculture 13 (2023) 1936.

[6] C.C. Baskin, J.M. Baskin, Seeds: Ecology, biogeography, and, evolution of dormancy and germination, BSeeds Ecol. Biogeogr. Evol. Dormancy Germination (2014), https://doi.org/10.1016/C2013-0-00597-X.

[7] J.D. Bewley, K.J. Bradford, H.W.M. Hilhorst, H. Nonogaki, Seeds: physiology of development, germination and dormancy, 3rd edition, 3rd Edition, Seeds: Physiol. Dev., Germination Dormancy (2013), https://doi.org/10.1007/978-1-4614-4693-4.

[8] M. Bloomberg, J.R. Sedcole, E.G. Mason, G. Buchan, Hydrothermal time germination models for radiata pine (Pinus radiata D. Don), Seed Sci. Res. (2009) 19, https://doi.org/10.1017/S0960258509990031.

[9] K.J. Bradford, A water relations analysis of seed germination rates, Plant Physiol. 94 (1990) 840–849, https://doi.org/10.1104/pp.94.2.840.

[10] K.J. Bradford, Applications of hydrothermal time to quantifying and modeling seed germination and dormancy, Weed Sci. (2002) 50, https://doi.org/10.1614/0043-1745(2002)050[0248:aohttq]2.0.co;2.

[11] K.J. Bradford, P. Bello, Applying population-based threshold models to quantify and improve seed quality attributes. Chapter from: Buitink, Julia, and Olivier Leprince, eds. Advances in seed science and technology for more sustainable crop production, Burleigh Dodds Sci. Publ. Ltd. (2022) 348.

[12] S. Caronni, R. Gentili, C. Montagnani, S. Citterio, Subpollen particle release from different species of the invasive allergenic genus Ambrosia: the effect of rainwater composition and wind speed, Aerobiologia (2021) 37, https://doi.org/10.1007/s10453-021-09722-7.

[13] B.S. Chauhan, H.H. Ali, S. Florentine, Seed germination ecology of Bidens pilosa and its implications for weed management, Sci. Rep. (2019) 9, https://doi.org/10.1038/s41598-019-52620-9.

[14] S. Del Vecchio, E. Mattana, T. Ulian, G. Buffa, Functional seed traits and germination patterns predict species coexistence in Northeast Mediterranean foredune communities, Ann. Bot. (2021) 127, https://doi.org/10.1093/aob/mcaa186.

[15] Finch-Savage, W.E., 2004. The use of population-based threshold models to descrine and predict the effects of seedbed environment on germination and seedling emergence of crops. Handb. seed Physiol. Appl. to Agric.

[16] J.J. Fu, J. Liu, L.Y. Yang, Y.J. Miao, Y.F. Xu, Effects of low temperature on seed germination, early seedling growth and antioxidant systems of the wild Elymus nutans Griseb, J. Agric Sci. Technol. (2017) 19.

[17] R.J. Gummerson, The effect of constant temperatures and osmotic potentials on the germination of sugar beet, J. Exp. Bot. (1986) 37, https://doi.org/10.1093/jxb/37.6.729.

[18] F.R. Hay, A. Mead, M. Bloomberg, Modelling seed germination in response to continuous variables: use and limitations of probit analysis and alternative approaches, Seed Sci. Res. (2014) 24, https://doi.org/10.1017/S096025851400021X.

[19] P.N. Hills, J. Van Staden, Thermoinhibition of seed germination, South Afr. J. Bot. (2003), https://doi.org/10.1016/S0254-6299(15)30281-7.

[20] E.O. Jalili, F. Ganj Abadi, O. Sharifi, J. Karkhane, Nalchegar, M.M. M, Introduction of flora, diversity and distribution of weeds in the micro climatic areas of Eshtehard County during 2013-2018, Iran. J. Weed Sci. 15 (2019) 41–57.

[21] S. Liu, K.J. Bradford, Z. Huang, D.L. Venable, Hydrothermal sensitivities of seed populations underlie fluctuations of dormancy states in an annual plant community, Ecology (2020) 101, https://doi.org/10.1002/ecy.2958.

[22] S.A. Lorestani, M. Oveisi, Alizadeh, R.M.H. H, Critical time of cutting after fruit development to prevent germination of Swallow wort (Cynanchum acutum L.) seeds, Iran. J. Weed Sci. (2021) 17.

[23] B. Manz, K. Müller, B. Kucera, F. Volke, G. Leubner-Metzger, Water uptake and distribution in germinating tobacco seeds investigated in vivo by nuclear magnetic resonance imaging, Plant Physiol. (2005) 138, https://doi.org/10.1104/pp.105.061663.

[24] R. Matuszak-Slamani, R. Bejger, M. Włodarczyk, D. Kulpa, M. Sienkiewicz, D. Gołębiowska, E. Skórska, A. Ukalska-Jaruga, Effect of humic acids on soybean seedling growth under polyethylene-glycol-6000-induced drought stress, Agronomy (2022) 12, https://doi.org/10.3390/agronomy12051109.

[25] F. Meighani, M.R. Karaminejad, Z. Farrokhi, Invasive weed swallow-wort (Cynanchum acutum L.) response to chemical and mechanical practices, Weed Biol. Manag. (2021) 21, https://doi.org/10.1111/wbm.12231.

[26] B.E. Michel, M.R. Kaufmann, The osmotic potential of polyethylene glycol 6000, Plant Physiol. (1973) 51, https://doi.org/10.1104/pp.51.5.914.

[27] P. Mishra, R. Dubey, Efect of aluminium on metabolism of starch and sugars in growing rice seedlings, Acta Physiol. Plant. 30 (2008) 265–275.

[28] E. Moltchanova, S. Sharifiamina, D.J. Moot, A. Shayanfar, M. Bloomberg, Comparison of three different statistical approaches (non-linear least-squares regression, survival analysis and Bayesian inference) in their usefulness for estimating hydrothermal time models of seed germination, Seed Sci. Res. (2020) 30, https://doi.org/10.1017/S0960258520000082.

[29] A. Moradi, B. Hamzehee, Bidens frondosa L.(Asteraceae), a new record for the flora of Iran, Iran. J. Bot. 27 (2021) 106–108.
[30] A. Muscolo, M. Sidari, U. Anastasi, C. Santonoceto, A. Maggio, Effect of PEG-induced drought stress on seed germination of four lentil genotypes, J. Plant Interact. (2014) 9, https://doi.org/10.1080/17429145.2013.835880.
[31] A. Onofri, P. Benincasa, M.B. Mesgaran, C. Ritz, Hydrothermal-time-to-event models for seed germination, Eur. J. Agron. (2018) 101, https://doi.org/10.1016/j.eja.2018.08.011.
[32] A.H. Pahlevani, F. Maighany, M.H. Rashed, M.A. Baghestani, M. Nassiri, M.T. Aleebrahim, Seed germination behavior of swallow wort (Cynanchum acutum, Iran. J. F. Crop. Res. 5 (2007) 47–52.
[33] C. Reynolds, G.S. Cumming, Seed dispersal by waterbirds in southern Africa: comparing the roles of ectozoochory and endozoochory, Freshw. Biol. (2016) 61, https://doi.org/10.1111/fwb.12709.
[34] J.P. Ribeiro-Oliveira, M.A. Ranal, M.A. Boselli, Water dynamics on germinating diaspores: physiological perspectives from biophysical measurements, Plant Phenomics (2020) 2020, https://doi.org/10.34133/2020/5196176.
[35] Ritz, C., Strebig, J.C., & Ritz, M.C. (2016). Package 'drc'. *Creative Commons: Mountain View, CA, USA* .
[36] H.R. Rowse, W.E. Finch-Savage, Hydrothermal threshold models can describe the germination response of carrot (Daucus carota) and onion (Allium cepa) seed populations across both sub- and supra-optimal temperatures, N. Phytol. (2003) 158, https://doi.org/10.1046/j.1469-8137.2003.00707.x.
[37] RStudio Team, 2020. RStudio: Integrated development environment for R. J. Wildl. Manage.
[38] Sadeghnejad, N. (2022)., 2022. Ecophysiology and control of Ambrosia psilostachya L.,. PhD Thesis, Univ. Tehran 192.
[39] P. Shimi, Survey of Swallow-wort (Cynanchum acutum) Control in Pistachio Orchards of Kerman Province, Iran. J. Weed Sci. 8 (2013) 53–62.
[40] S. Sohrabi, J. Pergl, P. Pyšek, L.C. Foxcroft, J. Gherekhloo, Quantifying the potential impact of alien plants of Iran using the Generic Impact Scoring System (GISS) and Environmental Impact Classification for Alien Taxa (EICAT), Biol. Invasions (2021) 23, https://doi.org/10.1007/s10530-021-02515-6.
[41] E. Soltani, C.C. Baskin, J.L. Gonzalez-Andujar, An overview of environmental cues that affect germination of nondormant seeds, Seeds (2022) 1, https://doi.org/10.3390/seeds1020013.
[42] S. Tokasi, E. Kazerooni Monfared, B. YaghoubI, M. Oveisi, H. Sasanfar, H. RahimianMashhadi, M.-S.H, First report of Ambrosia psilostachya L. from Iran: An invasive plant species establishing in coastal area of Gilan province (N Iran), Rostaniha 18 (2017) 222–226.
[43] S.Z. Tóth, G. Schansker, J. Kissimon, L. Kovács, G. Garab, R.J. Strasser, Biophysical studies of photosystem II-related recovery processes after a heat pulse in barley seedlings (Hordeum vulgare L.), J. Plant Physiol. (2005) 162, https://doi.org/10.1016/j.jplph.2004.06.010.
[44] T. Urbanova, L.G, Gibberellins and seed germination, Annu. Plant Rev. Gibberellins 49 (2016) 253–284.
[45] N. Verguet, L. Mondange, F. Nolent, A. Depeille, A. Garnier, F. Neulat-Ripoll, O. Gorgé, J.N. Tournier, Assessment of calcium hypochlorite for Bacillus anthracis spore surface's decontamination, Res. Microbiol. (2023) 174, https://doi.org/10.1016/j.resmic.2023.104053.
[46] R.L. Wang, Z.L. Feng, X.T. Liang, W.B. Xu, Y.J. Su, Y.Y. Song, R.S. Zeng, Comparative allelopathic and competitive abilities of 3-native forage legumes and the invasive weed Bidens pilosa L. Allelopath, J (2012) 29.
[47] M.S. Watt, M. Bloomberg, Key features of the seed germination response to high temperatures, N. Phytol. (2012), https://doi.org/10.1111/j.1469-8137.2012.04280.x.
[48] E. Wolny, A. Betekhtin, M. Rojek, A. Braszewska-Zalewska, J. Lusinska, R. Hasterok, Germination and the early stages of seedling development in Brachypodium distachyon, Int. J. Mol. Sci. (2018) 19, https://doi.org/10.3390/ijms19102916.
[49] G. Zhou, Q. Wang, A new nonlinear method for calculating growing degree days, Sci. Rep. (2018) 8, https://doi.org/10.1038/s41598-018-28392-z.